

RESCEU-36/98
 UTAP-296/98
 ADAC-030
 astro-ph/9810247

Reconstructing the radial profiles
 of gas density and temperature in clusters of galaxies
 from high-resolution X-ray and radio observations

Kohji Yoshikawa

Department of Astronomy, Kyoto University, Kyoto 606-8502, Japan.

and

Yasushi Suto

Department of Physics and Research Center for the Early Universe (RESCEU)

School of Science, University of Tokyo, Tokyo 113-0033, Japan.

e-mail: kohji@kusastro.kyoto-u.ac.jp, suto@phys.s.u-tokyo.ac.jp

ABSTRACT

We describe a non-parametric method to reconstruct gas density and temperature profiles of galaxy clusters from observations of X-ray surface brightness, emission-weighted temperature and the y -parameter through the Sunyaev-Zel'dovich effect. This method is based on the inversion of the projected profiles under the spherically symmetric approximation, which is independent of the equation of state of cluster gas and does not assume that the gas is in hydrostatic equilibrium. In particular we examine the reliability of the reconstruction method assuming a few theoretical models for cluster gas and assigning the statistical errors expected for future X-ray and radio observations. We also discuss briefly the effect of non-sphericity on the basis of simulated clusters.

Subject headings: cosmology: theory – dark matter – galaxies: clusters: general – X-rays: galaxies

The Astrophysical Journal Part 1, in press

1. Introduction

The importance of cluster abundances and baryon fractions is well-recognized and they are now regarded as one of the standard established statistics to constrain the cosmological models (e.g., Henry & Arnaud 1991; White, Efstathiou, & Frenk 1993; White et al. 1993; Viana & Liddle 1996; Eke, Cole, & Frenk 1996; Kitayama & Suto 1997; Kitayama, Sasaki & Suto 1998; Shimasaku 1998). On observational sides, the accuracy and reliability of such statistics will be considerably improved with several upcoming projects. In particular the angular resolutions of the AXAF (Advanced X-ray Astrophysics Facility) and XMM (X-Ray Multi-Mirror Mission) are $0.5''$ in 0.1-10 keV and $15''$ in 0.1-15 keV, respectively, and therefore they are expected to provide high-resolution X-ray surface brightness and temperature maps for many clusters with unprecedented angular and energy resolutions. The existing interferometric facilities in radio bands including BIMA (Berkeley Illinois Maryland Association) and OVRO (Owens Valley Radio Observatory) (e.g., Cooray et al. 1998) also produce two-dimensional maps of clusters via the Sunyaev-Zel'dovich (SZ) effect with $10'' \sim 30''$ resolution and signal-to-noise ratio more than 20. Furthermore, the Japanese Large Millimeter and Submillimeter Array (*LMSA*) project, for instance, will start an extensive survey of clusters in millimeter and submillimeter bands (see also Komatsu et al. 1998). Such detailed information of intracluster gas in multi-bands will significantly improve the role of clusters as cosmological probes.

On theoretical sides, recent N-body/hydrodynamical simulations (e.g., Couchman et al. 1995; Bryan & Norman 1998; Eke & Frenk 1998; Yoshikawa, Itoh, & Suto 1998) start to reveal several important keys to understanding the intracluster gas on a physical basis. In particular, Navarro, Frenk & White (1997; NFW hereafter) suggest that a dark matter halo of cluster is described by a universal density profile, or at least by a class of well-specified functional forms (see Fukushige & Makino 1997; Moore et al. 1998). Their results imply that with appropriate equation of state, the gas density and temperature profiles of clusters can be predicted given a cosmological model, at least in a spherically symmetric approximation (Makino, Sasaki & Suto 1998; Suto, Sasaki, & Makino 1998). In other words, one does not have to adopt too simplified empirical models like the isothermal β -model in approximating the cluster gas. In fact we are now in a position to construct a more physical model combining the new observational data and the theoretical predictions. By reconstructing the cluster profiles in a model-independent manner from the observations and comparing them with the theoretical models, one can directly test the universal dark halo conjecture, and if confirmed, probe the cosmological parameters in an independent and complementary manner with more conventional approaches like cluster abundances, cosmic microwave background anisotropies, and galaxy clustering statistics (e.g., Tegmark et al. 1998). Therefore a reliable and model-independent reconstruction of radial profiles of cluster gas should also contribute significantly to the conventional analyses of clusters including the estimates of the Hubble constant (Silk & White 1978; Inagaki, Sugino, & Suto 1995; Kobayashi, Sasaki & Suto 1996) and peculiar velocity (e.g., Yoshikawa, Itoh, & Suto 1998), baryon fraction and gravitational lensing (e.g., Wu & Fang 1997). See Birkinshaw (1998) for an excellent review on the SZ effect and its cosmological implications.

In this paper, we apply an idea proposed earlier by Silk & White (1978), and examine in detail a non-parametric reconstruction method of the radial profiles of clusters, which does not depend on any assumption such as hydrostatic equilibrium and equation of state of cluster gas except for the spherical symmetry of clusters. We also propose a new method to reconstruct the temperature radial profile of clusters only from X-ray observations. This method is also applicable to other elliptic models as well, provided that the ellipticity is assumed a priori (c.f., Fabricant, Rybicki & Gorenstein 1984; Hughes & Birkinshaw 1998). In this context, we note that Zaroubi et al. (1998) recently proposed a different reconstruction method of 3-dimensional profiles of clusters using the Fourier Slice Theorem, and our current scientific motivation is quite similar with theirs. While their method, employing Fourier transform of the projected images and inverse transformation, is fairly complicated and it is not clear yet to what extent it is practical, our procedure is rather straightforward and useful.

2. Abel's integral solution for radial profiles of gas density and temperature in clusters of galaxies

Most observable quantities for a cluster are often written as an integration over the line-of-sight:

$$f(\theta) = \int_{-\infty}^{\infty} g(r) dl = 2 \int_{d_A \theta}^{\infty} g(r) \frac{r dr}{\sqrt{r^2 - d_A^2 \theta^2}}, \quad (1)$$

where the cluster is assumed to be spherically symmetric, θ and r denote the (projected) angular separation and (3D) spatial radius from the cluster center, and d_A is the angular diameter distance to the cluster. Using Abel's integral, equation (1) can be inverted to give

$$g(r) = \frac{1}{\pi d_A} \int_{\infty}^{r/d_A} \frac{df(\theta)}{d\theta} \frac{d\theta}{\sqrt{\theta^2 - r^2/d_A^2}}. \quad (2)$$

The above Abel's integral solution can be readily applied to the bolometric X-ray surface brightness:

$$S_x(\theta) = A_x \int_{-\infty}^{\infty} \alpha_X(T_e) n_e^2(\sqrt{\theta^2 d_A^2(z) + l^2}) dl = 2A_x \int_{d_A \theta}^{\infty} \alpha_X(T_e) n_e^2(r) \frac{r dr}{\sqrt{r^2 - d_A^2 \theta^2}}, \quad (3)$$

and y-parameter, or more generally, the SZ flux at a given frequency band:

$$S_y(\theta) = 2A_y \int_{d_A \theta}^{\infty} T_e(r) n_e(r) \frac{r dr}{\sqrt{r^2 - d_A^2 \theta^2}}. \quad (4)$$

In the above expressions, $T_e(r)$ and $n_e(r)$ are the temperature and number density of the electron gas of the cluster, and $\alpha_X(T_e)$ is the X-ray emissivity. While the coefficients A_x and A_y can be explicitly computed once the observational bands are specified, their specific

values are not important in the following analysis. Silk & White (1978) were the first to propose to apply the Abel inversion to the X-ray and SZ profiles, but their discussion is limited to the estimation of the central values of gas density and temperature aiming at the determination of $d_A(z)$. The purpose of the present paper is to examine the feasibility of the reconstruction method quantitatively, properly taking account of the current and upcoming data quality.

If one considers only the thermal bremsstrahlung for the X-ray emissivity, which is a good approximation for clusters with $T_e \gtrsim 3\text{keV}$, then $\alpha_X(T_e) = T_e^{1/2}(r)$, and equations (3) and (4) are inverted to yield

$$[n_e(r)]^3 = \frac{A_y}{\pi A_x^2 d_A} \frac{\left[\int_{\infty}^{r/d_A} \frac{dS_x(\theta)}{d\theta} \frac{d\theta}{\sqrt{\theta^2 - r^2/d_A^2}} \right]^2}{\int_{\infty}^{r/d_A} \frac{dS_y(\theta)}{d\theta} \frac{d\theta}{\sqrt{\theta^2 - r^2/d_A^2}}}, \quad (5)$$

$$[T_e(r)]^2 / \alpha(T_e) = [T_e(r)]^{3/2} = \frac{A_x}{\pi A_y^2 d_A} \frac{\left[\int_{\infty}^{r/d_A} \frac{dS_y(\theta)}{d\theta} \frac{d\theta}{\sqrt{\theta^2 - r^2/d_A^2}} \right]^2}{\int_{\infty}^{r/d_A} \frac{dS_x(\theta)}{d\theta} \frac{d\theta}{\sqrt{\theta^2 - r^2/d_A^2}}}. \quad (6)$$

In reality, the observed X-ray flux is band-limited and one should also take into account other emission processes than the thermal bremsstrahlung. While the present methodology works for those cases, the result cannot be expressed in a simple form as the above equation, and we focus on the case of $\alpha_X(T_e) = T_e^{1/2}(r)$ as an explicit example.

If the emission-weighted temperature profile projected on the sky:

$$T_X(\theta) \equiv \frac{\int_{-\infty}^{\infty} T_e \alpha_X(T_e) n_e^2(\sqrt{d_A^2 \theta^2 + l^2}) dl}{\int_{-\infty}^{\infty} \alpha_X(T_e) n_e^2(\sqrt{d_A^2 \theta^2 + l^2}) dl} = \frac{\int_{-\infty}^{\infty} T_e \alpha_X(T_e) n_e^2(\sqrt{d_A^2 \theta^2 + l^2}) dl}{S_x(\theta)/A_x}, \quad (7)$$

is measured, however, one can similarly derive

$$T_e(r) \alpha_X(T_e) [n_e(r)]^2 = \frac{1}{\pi A_x d_A} \int_{\infty}^{r/d_A} \frac{d[S_x(\theta) T_X(\theta)]}{d\theta} \frac{d\theta}{\sqrt{\theta^2 - r^2/d_A^2}}. \quad (8)$$

Combining with Abel's integral solution of equation (3):

$$\alpha_X(T_e) [n_e(r)]^2 = \frac{1}{\pi A_y d_A} \int_{\infty}^{r/d_A} \frac{dS_x}{d\theta} \frac{d\theta}{\sqrt{\theta^2 - (r/d_A)^2}}, \quad (9)$$

one can obtain the temperature profile $T_e(r)$ by

$$T_e(r) = \frac{\int_{\infty}^{r/d_A} \frac{d[S_x(\theta)T_X(\theta)]}{d\theta} \frac{d\theta}{\sqrt{\theta^2 - r^2/d_A^2}}}{\int_{\infty}^{r/d_A} \frac{dS_x}{d\theta} \frac{d\theta}{\sqrt{\theta^2 - (r/d_A)^2}}}. \quad (10)$$

Equation 10 is more suitable for reconstructing the temperature profile than equation (6) in that all the necessary information can be obtained from the X-ray observation alone, and that it is independent of the specific form of the X-ray emissivity $\alpha_X(T_e)$. The use of equation (7) requires sufficiently good spatial and energy resolutions, both of which are feasible only with future X-ray satellites including AXAF and XMM.

All the above procedures (eqs.[5], [6] and [10]) involve the integral of the form:

$$\int_{\infty}^{r/d_A} \frac{df(\theta)}{d\theta} \frac{d\theta}{\sqrt{\theta^2 - (r/d_A)^2}}. \quad (11)$$

In what follows we numerically evaluate the integral as

$$\sum_{i=i_{\min}}^{i_{\max}} \frac{f_i - f_{i+1}}{\sqrt{\theta_{i+\frac{1}{2}}^2 - (r/d_A)^2}}, \quad (12)$$

where the observed quantity f_i ($i = 1, i_{\max}$) is given at the discrete angular radius θ_i , and $\theta_{i+\frac{1}{2}} = (\theta_i + \theta_{i+1})/2$. i_{\max} is the index for the outermost bin and i_{\min} indicates the bin which corresponds to r/d_A . In practice we adopt $i_{\max} = 30$ for definiteness. In fact one could improve the above evaluation by *pre-smoothing* the dataset to reduce the discrete noise component. While such a procedure is inevitably model-dependent and we did not attempt one in what follows, this would be practically useful in dealing with the actual observational data and improve the results below.

3. Statistical and systematic errors in the reconstruction

3.1. models of gas density and temperature profiles

Strictly speaking one needs to observe $S_x(\theta)$ and $S_y(\theta)$ for $r/d_A < \theta < \infty$ in order to determine $n_e(r)$ and $T_e(r)$. In practice, however, the observable fluxes are limited to the finite extent of clusters, and also contaminated by the angular resolution of the telescope and the detector noise especially at outer regions. Moreover realistic clusters are not spherically symmetric to some degree. In this section, we employ several cluster models with different density and temperature profiles, and examine how the above reconstruction method works in taking account of such observational limitations. More specifically, we examine the following four models:

Model A: this is a conventional isothermal β -model described by

$$n_e(r) = \frac{n_{e0}}{[1 + (r/r_c)^2]^{3\beta/2}}, \quad T_e(r) = T_{e0}. \quad (13)$$

We adopt a typical value for clusters, $\beta = 2/3$, for definiteness. The values of the other parameters, n_{e0} , T_{e0} , and r_c , are irrelevant for our current purpose since all the results can be rescaled appropriately.

Model B: consider a family of the dark matter halo profiles given by

$$\rho_{\text{DM}}(x) = \frac{\delta_{\text{DM}}}{x^\mu(1+x^\nu)^\lambda}, \quad (14)$$

where $x \equiv r/r_s$ is the dimensionless radius in units of the characteristic scale r_s , and δ_{DM} is the amplitude of the profile. NFW claimed that a halo profile with $(\mu, \nu, \lambda) = (1, 2, 1)$ is the universal shape fairly independent of the cosmological initial conditions (see also Fukushige & Makino 1997 and Moore et al. 1998).

Suto, Sasaki & Makino (1998) found an analytical solution for the gas density and temperature profiles when the gas obeys the polytropic equation of state $T_e(r) = T_{e0}[n_e(r)/n_{e0}]^{1/n}$ and its self-gravity can be neglected compared with the dark halo. Their solution is written as

$$n_e(r) = n_{e0}[1 - B_p f(x)]^n, \quad T_e(r) = T_{e0}[1 - B_p f(x)], \quad (15)$$

where

$$f(x) \equiv \int_0^x \frac{u^{1-\mu}}{(1+u^\nu)^\lambda} du - \frac{1}{x} \int_0^x \frac{u^{2-\mu}}{(1+u^\nu)^\lambda} du, \quad (16)$$

$$B_p \equiv \frac{4\pi G}{n+1} \frac{\mu_g m_p \delta_{\text{DM}} r_s^2}{k T_{e0}}, \quad (17)$$

G is the gravitational constant, k is the Boltzmann constant, μ_g is the mean molecular weight of the gas, and m_p is the proton mass.

Therefore given the dark matter halo profile, the gas density and temperature profiles are specified by the additional two parameters n and B_p . We consider the following two models (model B and C) which have the analytic solutions for $f(x)$. In the NFW model ($\mu = 1$, $\nu = 2$, and $\lambda = 1$),

$$f(x) = 1 - \frac{\ln(1+x)}{x}. \quad (18)$$

We adopt $n = 12$, $B_p = 1.0$ for model B so that the resulting $S_x(\theta)$ has a fairly similar profile to that of model A (corresponding to $\beta = 2/3$).

Model C: halo model with $\mu = 3/2$, $\nu = 1$, and $\lambda = 3/2$ has

$$f(x) = 2\sqrt{\frac{1+x}{x}} - \frac{2}{x} \ln \left(\sqrt{x} + \sqrt{1+x} \right). \quad (19)$$

We adopt $n = 11$, $B_p = 0.5$, again so that the resulting $S_x(\theta)$ resembles the profile of model A.

Model D: we select a simulated cluster (cluster A at $z = 0$ in Yoshikawa, Itoh, & Suto 1998) in order to examine a possible effect of the non-sphericity. The cluster has lower temperature in the central region unlike the above three models; in this sense also, it can be regarded as a good example to test the robustness of the present reconstruction method. In practice, we find that the circularly averaged profiles of its X-ray and SZ surface brightness of the cluster are well approximated by

$$S_x(\theta) = \frac{S_x(0)}{[1 + (d_A \theta / r_X)^2]^{3\beta_X - 1/2}}, \quad S_y(\theta) = \frac{S_y(0)}{[1 + (d_A \theta / r_y)^2]^{3\beta_y/2 - 1/2}}, \quad (20)$$

with $\beta_X = 0.69$, $r_X = 0.13\text{Mpc}$, $\beta_y = 0.86$, and $r_y = 0.18\text{Mpc}$. Therefore we adopt the above spherical fits (with appropriate errors; see the next subsection) as input data, and examine the extent to which the reconstructed density and temperature profiles agree with the spherically averaged ones directly computed from the simulated data.

3.2. error assignment and reconstructed profiles

Figure 1 shows the input projected profiles of bolometric X-ray flux, y-parameter and X-ray emission-weighted temperature (eqs. [3], [4], and [7]) for models A to D described in §3.1. In order to estimate statistical and possible systematic errors to our method due to observational uncertainties and deviation from spherical symmetry, we perform the reconstruction after adding the following Gaussian distributed errors. More specifically we examine models A, B, and C to estimate errors from observational uncertainties, and model D from the deviation from spherical symmetry.

The relevance of the error assignment should sensitively depend on both the observing facilities and the specific target clusters one has in mind. For models A to C, we consider two cases (I and II) for error assignment; for S_x the assumed errors are fairly realistic even with the current X-ray satellites (e.g., Briel & Henry 1996) at least for relatively near and bright clusters, but for S_y and T_X the errors should be feasible only with the future interferometer facilities including Japanese LMSA (Large Millimeter and Submillimeter Array; Kawabe, private communication), and future X-ray satellites with high sensitivity such as XMM with sufficiently large integration time. For a given error of S_x , one may roughly scale the resulting error-bars in Figure 2 for the different level of the errors in S_y and T_X . With this in mind, we consider two specific cases; for the case I, we assign the 1σ errors as

$$\Delta S_x(\theta) = 10^{-4} S_x(0), \quad \Delta S_y(\theta) = 10^{-2} S_y(0), \quad \Delta T_X(\theta) = 10^{-2} T_X(\theta) \quad (21)$$

at each θ , and for the case II they are

$$\Delta S_x(\theta) = 10^{-3} S_x(0), \quad \Delta S_y(\theta) = 2 \times 10^{-2} S_y(0), \quad \Delta T_X(\theta) = 5 \times 10^{-2} T_X(\theta). \quad (22)$$

Error bars in Figure 1 indicate those 1σ dispersion of Gaussian errors in the case of I and II (all the curves for case I are artificially shifted upward so that the two cases are easily distinguished). For model D, on the other hand, we assign the 1σ dispersion of the fluxes around the circularly averaged values directly computed from simulation data profile by Yoshikawa, Itoh, & Suto (1998), and do not attempt to include the observational errors. We sample the data using 30 radial bins in logarithmically equal intervals.

According to the above procedure, we construct 200 realizations for each model with different random number for the error assignment, and then perform the reconstruction. Figure 2 shows the reconstructed profiles of gas density (top panels), the ratio between them (upper middle panels), temperature (lower middle and bottom panels) for each model. The lower middle panels show the temperature profiles reconstructed from X-ray surface brightness and the SZ flux (eq. [6]) and the bottom panels show that reconstructed from X-ray surface brightness and emission-weighted temperature (eq.[10]). Solid lines correspond to the *true* profiles for models A to C (again the results for case I are artificially shifted upward for an illustrative purpose), and the spherically averaged profiles for model D.

The reconstructed profiles are plotted with their 1σ error-bars computed from the 200 realizations. Since the main contribution for the projected fluxes comes from the radius around r_c , the estimates become less reliable either for $r \ll r_c$ or $r \gg r_c$. Also the reconstruction works better for $n_e(r)$ than for $T_e(r)$ since the X-ray emissivity is more sensitive to the former ($\propto n_e^2 T_e^{1/2}$ for the thermal bremsstrahlung). The upper and lower solid lines in model D represent the $\pm 1\sigma$ deviation from the spherically averaged profile, which illustrate the degree of non-sphericity of the simulated cluster. The degree of asphericity in our simulated cluster is comparable to, or even larger than, the error due to the reconstruction procedure. Since our simulated cluster seems to be typical in the light of the distribution of non-sphericity in the observed cluster sample (Mohr et al. 1995), the non-sphericity of that degree does not seriously degrade the current methodology although the inclusion of non-spherical effect is definitely an important next step (Zaroubi et al. 1998).

4. Discussion and conclusions

We have presented a method to reconstruct the radial profiles of gas density and temperature in clusters of galaxies. Since most existing techniques start with some sort of empirical cluster gas profile and attempt to find the best-fit in that modeling, the result is fairly model-dependent. Our current method is in marked contrast to the previous ones in that the radial profiles can be reconstructed in a non-parametric manner without assuming the equation of state or hydrostatic equilibrium of cluster gas if high-resolution projected profiles of X-ray and SZ observations are given.

We apply this method to three analytic spherical models (A to C) with gas density and temperature profiles and one non-spherical simulated cluster. For models A to C, the fractional uncertainties of reconstructed gas density profiles are less than 1% in our case I

while they amount to 20–30% at central regions and 2–3% at outer regions in our case II. On the other hand, the estimate of temperature is sensitive to the accuracy of the SZ flux or X-ray emission weighted temperature as in Figure 2. With the degree of asphericity in our simulated cluster, the resulting systematic error is smaller than our adopted statistical errors. In fact while our error assignment for X-ray temperature and the SZ fluxes may be rather optimistic, one can rescale the resulting error bars according to the real observation if necessary.

Although we have presented the analysis on the basis of the spherical symmetry, the same methodology is in principle applicable to other non-spherical systems if one accepts some additional assumption on the density distribution along the line of sight. In this context, one of the most practically important ways is to assume a bilateral symmetry (e.g., Fabricant, Rybicki & Gorenstein 1984; Hughes & Birkinshaw 1998). In this case, all the results presented in this paper is readily applicable simply by an appropriate choice of the coordinate transformation.

Considering the future extensive observation of clusters of galaxies in X-ray and radio bands with upcoming facilities such as ABRIXAS, AXAF, XMM, and LMSA, high-resolution images of clusters of galaxies in X-ray and radio bands will be available with unprecedented high signal-to-noise ratio and the reconstruction of profiles of clusters of galaxies with sufficient accuracy should be feasible. More quantitative discussion of the error and the resulting accuracy of the reconstruction should definitely depend on the specific target cluster, and we are not able to proceed further at this moment. Nevertheless we believe that the current methodology becomes useful in near future. Furthermore with such a reliable reconstructed radial profiles of clusters of galaxies, even if feasible only for relatively near and bright ones, one can revisit various cosmological issues, in which simplified and/or empirical models have been adopted, including the estimates of Hubble constant (Kobayashi, Sasaki & Suto 1996), peculiar velocity of clusters of galaxies (Yoshikawa, Itoh, & Suto 1998), the $L - T$ relation which is inconsistent with observations if derived from a simple scaling argument, and physics cooling flow.

We thank Pat Henry for information of the current observational errors of the X-ray fluxes, and Ryohei Kawabe for useful discussion on the current and future observing facilities in radio, millimeter and submillimeter bands and their expected performance. We also thank an anonymous referee for several comments which helped improve the earlier version of the paper. Numerical computations were carried out on VPP300/16R and VX/4R at ADAC (the Astronomical Data Analysis Center) of the National Astronomical Observatory, Japan, as well as at RESCEU (Research Center for the Early Universe, University of Tokyo) and KEK (National Laboratory for High Energy Physics, Japan). This research was supported in part by the Grants-in-Aid by the Ministry of Education, Science, Sports and Culture of Japan (07CE2002) to RESCEU, and by the Supercomputer Project (No.97-22) of High Energy Accelerator Research Organization (KEK).

REFERENCES

Birkinshaw, M. 1998, Phys.Rep., in press (astro-ph/9808050).
Birkinshaw, M., Hughes, J.P. & Arnaud, K.A. 1991, ApJ, 379, 466
Briel, U.G., & Henry, J. P. 1996, ApJ, 472, 131
Bryan, G.L., & Norman, M. 1998, ApJ, 495, 80
Cooray, A.R., Grego, L., Holzapfel, W.L., Joy, M., & Carlstrom, J.E. 1998, AJ, 115, 1388
Couchman, H.M.P., Thomas, P.A. & Pearce, F.R. 1995, ApJ, 452, 797
Eke, V. R., Cole, S., & Frenk, C. S. 1996, MNRAS, 282, 263
Eke, V.R, Navarro, J.F., & Frenk, C.S. 1998, ApJ, 503, 569
Evrard, A. E., & Henry, J. P. 1991, ApJ, 383, 95
Fabricant, D., Rybicki, G., & Gorenstein, P. 1984, ApJ, 286, 186
Fukushige, T., & Makino, J. 1997, ApJ, 477, L9
Henry, J. P., & Arnaud, K. A. 1991, ApJ, 372, 410
Hughes, J.P., & Birkinshaw, M. 1998, ApJ, 501, 1
Inagaki, Y., Sugino, T., & Suto, Y. 1995, PASJ, 47, 411
Kitayama, T. & Suto, Y. 1997, ApJ, 490, 557
Kitayama, T., Sasaki, S., & Suto, Y. 1998, PASJ, 50, 1
Kobayashi, S., Sasaki, S., & Suto, Y. 1996, PASJ, 48, L107
Komatsu, E., Kitayama, T., Suto, Y., Hattori, M., Kawabe, R., Matsuo, H., Schindler, S., & Yoshikawa, K. 1998, Nature, submitted.
Makino, N., Sasaki, S., & Suto, Y. 1998, ApJ, 497, 555
Mohr, J.J., Evrard, A.E., Fabricant, D.G., & Geller, M.J. 1995, ApJ, 447, 8
Moore, B., Governato, F., Quinn, T., Stadel, J., & Lake, G. 1998, ApJ, 499, L5
Navarro, J.F., Frenk, C.S., & White, S.D.M. 1997, ApJ, 490, 493 (NFW)
Rephaeli, Y. 1995, ARA&A, 33, 541
Shimasaku, K. 1998, ApJ, 489, 501
Silk, J. & White, S.D.M. 1978, ApJ, 226, L103
Sunyaev R.A. & Zel'dovich Ya.B. 1972, Comments on Astrophys.& Space Phys., 4, 173
Sunyaev R.A. & Zel'dovich Ya.B. 1980, MNRAS, 190, 413
Suto, Y., Sasaki, S., & Makino, N. 1998, ApJ, 509, December 20 issue, in press
Tegmark, M., Eisenstein, D.J., Hu, W., & Kron, R. 1998, ApJ, in press
(astro-ph/9805117).
Viana, P. T. P., & Liddle, A. R. 1996, MNRAS, 281, 323
White, S. D. M., Efstathiou, G., & Frenk, C. S. 1993, MNRAS, 262, 1023
White, S. D. M., Navarro, J. F., Evrard, A. E., & Frenk, C. S. 1993, Nature, 366, 429
Wu, X.P., & Fang, L.Z. 1997, ApJ, 483, 62
Yoshikawa, K., Itoh, M., & Suto, Y. 1998, PASJ, 50, 203
Zaroubi, S., Squires, G., Hoffman, Y., Silk, J. 1998, ApJ, 500, L87

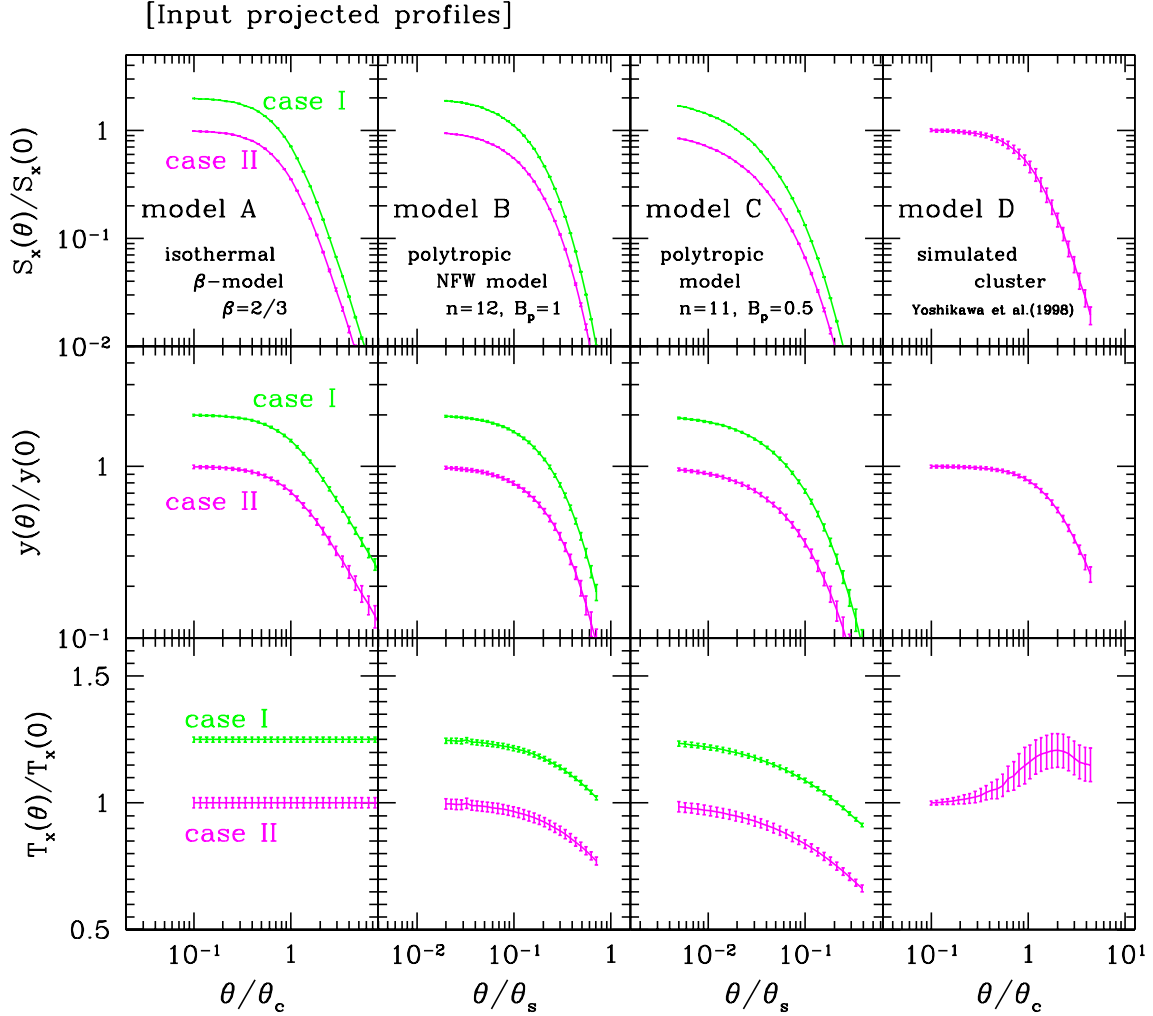


Fig. 1.— Input profiles of scaled X-ray surface brightness (upper panels), the SZ flux (middle panels) and emission-weighted temperature (lower panels) for models A to D. For models A, B, and C, the smaller and larger error bars correspond to our cases I and II of error assignment, respectively (eqs. [21] and [22]). The curves corresponding to case I are artificially shifted upward for an illustrative purpose. For model D, the error bars indicate the 1σ deviation from spherical symmetry obtained from the numerical simulation (Yoshikawa et al. 1998). The angular core radius θ_c in model D is computed from the core radius r_c of the β -model fit to the spherically averaged density profile of the simulated cluster. Solid lines indicate the true profile *before* assigning the error.

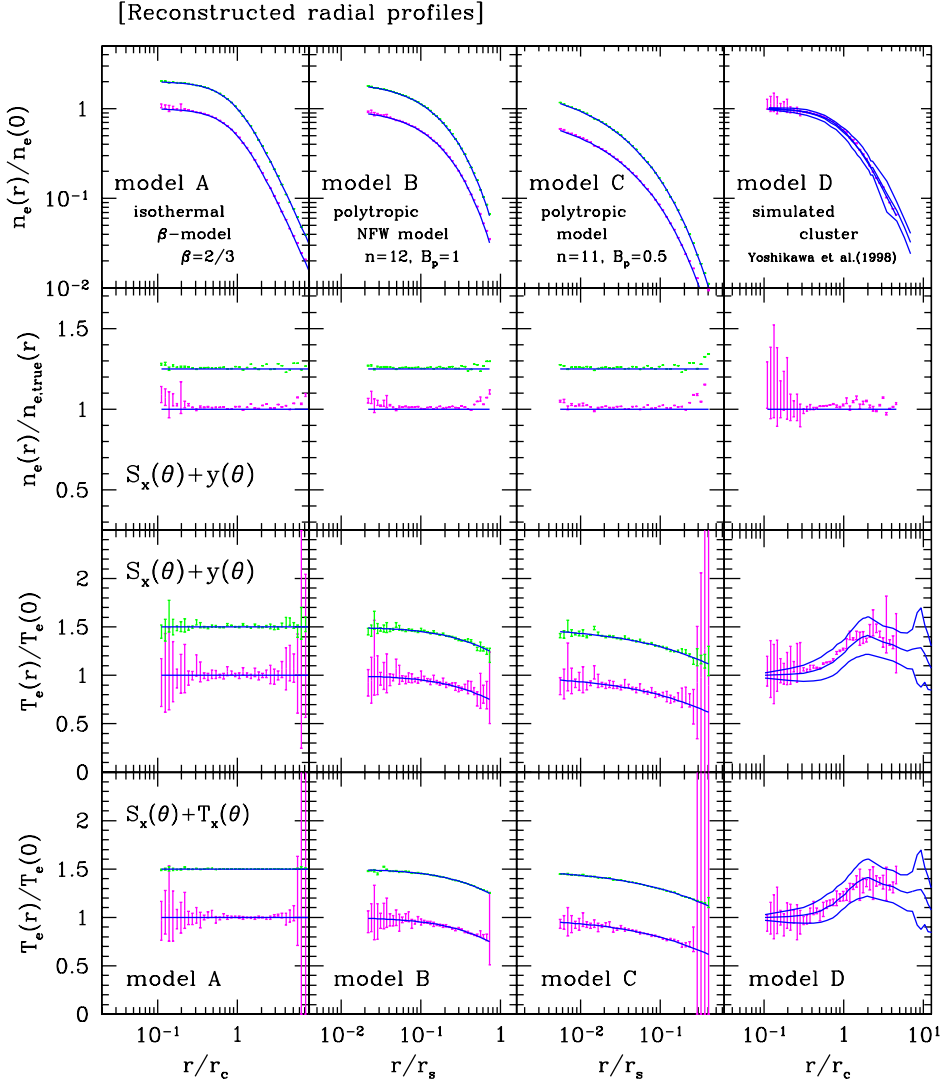


Fig. 2.— Reconstructed gas density and temperature profiles for models A to D. *Top panels*: reconstructed $n_e(r)$ in units of the central value; *Upper middle panels*: reconstructed $n_e(r)$ in units of the true density $n_{e,\text{true}}(r)$; *Lower middle panels*: $T_e(r)$ reconstructed with X-ray and SZ fluxes in units of the central value; *Bottom panels*: $T_e(r)$ reconstructed with X-ray flux and emission-weighted projected temperature in units of the central value. For models A to C, solid lines indicate the true model profile, and the error bars correspond to those shown in Figure 1. The curves corresponding to case I are artificially shifted upward for an illustrative purpose. For model D, the middle solid lines in each panel represent the spherically averaged profiles, and the upper and lower solid lines indicate the $\pm 1\sigma$ dispersion of the simulated cluster around the spherically averaged profile.